Wave propagation in mechanical metamaterials

Zhou, Y.; Zhou Y.

Citation

Zhou, Y. (2017, October 17). *Wave propagation in mechanical metamaterials*. *Casimir PhD Series*. Retrieved from https://hdl.handle.net/1887/56412

Cover Page

Universiteit Leiden

Author: Yujie Zhou
Title: Wave propagation in mechanical metamaterials
Date: 2017-10-17

Chapter 3

Topological rotor chains with impurities

I N T H I S C H A P T E R we investigate topological rotor chains with impurities. In Sec. 3.1, we examine how kinks and antikinks interact with a spring stiffness impurity in the lattice. In Sec. 3.2, we make a connection between linear mode analysis and nonlinear dynamics of kink motion in the context of spring length impurities.

3.1 Spring stiffness impurities

In this section we numerically explore whether the kink-antikink asymmetry also manifests in the way these excitations interact with a single lattice impurity, a natural starting point to study their propagation in disordered lattices. For the conventional ϕ^4 models, previous studies on kink-impurity interactions (in both discrete models [66] and continuum field models [67]) have shown that scattering can result in transmission, trapping or reflection of kinks, depending on the type of the impurity, the attraction/repulsion strength of the impurity and the kink's initial velocity. Although similar scattering also occurs in the topological rotor chain model, we also find other novel phenomena, for instance, the kink can split into two kinks and one antikink. Moreover as we will see, kinks and antikinks no longer scatter in the same way

– a feature which underscores the kink-antikink asymmetry in our topological rotor chain. Fig. 3.1 summarizes all the possible scattering scenarios that we observe. In this chapter, we study impurities in properties of the springs, which yield a richer set of effects on the response than mass impurities.
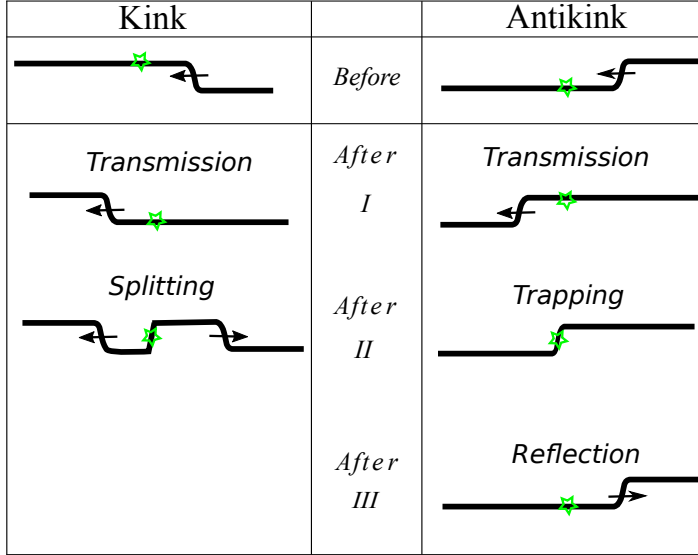
Kink		Antikink
	Before	
Transmission	*After* *I*	*Transmission*
Splitting	*After* *II*	*Trapping*
	After *III*	*Reflection*

Figure 3.1. Illustrated are the possible scenarios for how the kink and antikink interact with a single impurity of spring stiffness. As indicated by the arrow, an initial kink or antikink approaches the impurity site (indicated by the green star) from the right. After scattering, the incident kink is either: (**I**) perfectly transmitted or (**II**) splits into a reflected kink, a transmitted kink and an antikink that gets trapped at the impurity site. The incident antikink is either: (**I**) perfectly transmitted, (**II**) trapped at the impurity site or (**III**) perfectly reflected.

In this section, we model an impurity by changing the spring stiffness constant at a single site (Fig. 2.1a). We study a topological chain with lattice spacing $a = 1$ and rotor length $r/a = 0.8$ and with equillibirum angle $\bar{\theta} = 0.28$. We perform Newtonian dynamics simulation on a system with 60 rotors using free boundary conditions, and for a range of impurity spring stiffness constant k_i and kink/antikink initial velocity v_0. See Fig. 3.1 for a table of the possible scattering scenarios that we observe.

Consider first the kink-impurity interaction. For most k_i and v_0, the kink simply passes through the impurity and may excite an impurity mode, which can be seen in the form of small fluctuations in the middle of the chain as shown in Fig. 3.2a. When the impurity spring is sufficiently soft, the incident kink splits into three: a transmitted kink, an antikink that is trapped at the impurity and a reflected kink. This is shown in Fig. 3.2b.
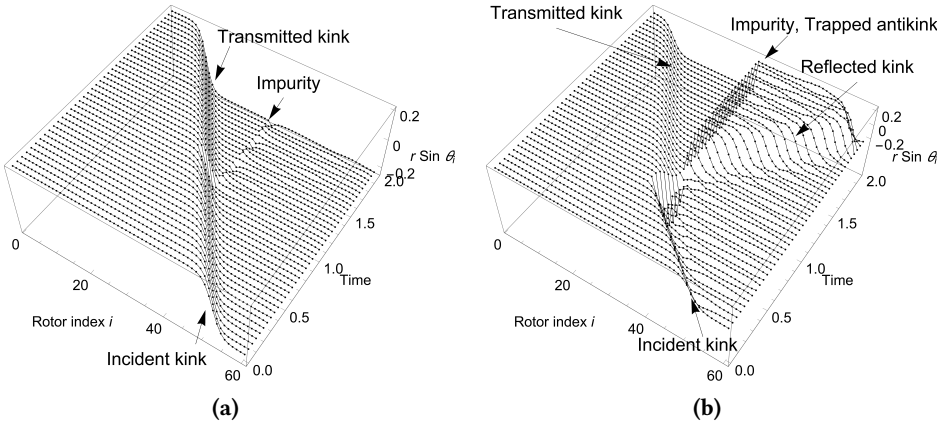

Figure 3.2. A kink interacts with an impurity (different spring stiffness) and is either (**a**) transmitted, shown here for $v_0 = 4.0$ and $k_i/k = 0.10$ or (**b**) splits into a transmitted kink, a reflected kink and an antikink trapped at the impurity, shown here for $v_0 = 9.6$ and $k_i/k = 0.01$. The non-dimensional parameters are $M = 1, k = 10000, r/a = 0.8, \bar{\theta} = 0.28$.

Antikink scattering results in an ever richer set of behaviors. Recall that the springs near the location of an antikink are always stretched significantly, see Fig. 2.4b. For k_i/k near 1, the antikink gets transmitted with energy dissipation and thus slows down (Fig. 3.3a). Softening the impurity spring stiffness creates an attractive potential well for the antikink. The antikink may then release a part of its potential energy and get trapped at such an impurity site (Fig. 3.3b). If the impurity spring is made even softer, such that an antikink can no longer transfer its kinetic energy forward or dissipate it sufficiently quickly to be trapped, the incident antikink is completely reflected (Fig. 3.3c). For similar reasons, a stiffer impurity acts like a repulsive potential
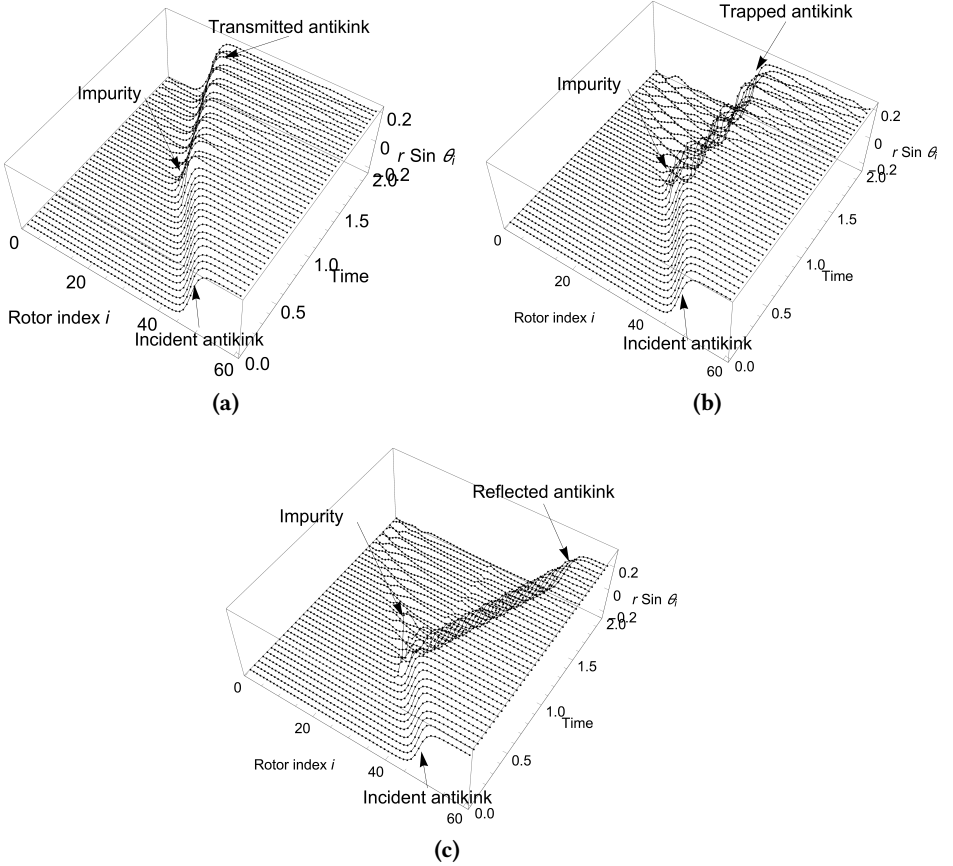
well that can reflect slow moving antikinks.

Figure 3.3. An antikink interacts with an impurity and is either **(a)** transmitted, shown here for $v_0 = 4.0$ and $k_i/k = 0.80$, **(b)** trapped, shown here for $v_0 = 4.0$ and $k_i/k = 0.70$ or **(c)** reflected, shown here for $v_0 = 4.8$ and $k_i/k = 0.20$. The system parameters are the same as Fig. 3.2.

These numerical results are summarized in the phase diagrams in the space of k_i and v_0 in Fig. 3.4. First, note that a kink (Fig. 3.4a) behaves quite differently from an antikink (Fig. 3.4b). For instance, a kink is never completely

trapped or reflected by an impurity. The reason is that it has zero intrinsic potential energy and thus, no potential energy to lose during a scattering event. As a collective object, the kink experiences a flat potential landscape along the chain. It will always go through the impurity, unless k_i is so soft or v_0 is so large that the initial kinetic energy of the kink is sufficient to stretch the impurity spring to form a pinned antikink. That is when scattering results in the kink being split. This also explains the positive slope of the boundary line between these two regimes. (The topological constraints of the field require that the number of kinks minus the number of antikinks remains constant [50], which is one for our boundary conditions.)

For an antikink, the scattering phase diagram has more regimes (Fig. 3.4b). The positive slope of the boundary curve at higher k_i between the upper reflection regime (square) and the transmission regime (circle) comes from the fact that the higher the barrier is, the faster the antikink needs to be, to get transmitted. The negative slope of the boundary between the transmission regime (circle) and the trapping regime (triangle), suggests that a softer impurity spring causes the antikink to dissipate more energy. The antikink then needs a sufficiently high initial velocity to avoid being trapped at such an impurity site. The positive slope of the curve between the trapped regime (triangle) and the lower reflection regime (square) suggests that if the impurity spring is so soft such that it can no longer transform the kinetic energy into other forms or channelize the kinetic energy to the other side of the impurity sufficiently "quickly", an antikink incident with sufficiently high energy will then be completely reflected. (In simulations we find that the maximum initial velocity with which we can launch an antikink is around $v_0 = 12$. Above this, the antikink itself becomes unstable and tends to quickly disintegrate.)

For the topological rotor chain, the antikink scattering behaviour is therefore very similar to the ones reported for kinks and antikinks in previous studies on the ϕ^4 model [66, 67]. In addition, for normal ϕ^4 kinks and antikinks, one also observes resonance windows which are alternating regimes of the excitation being reflected or trapped, along the axis of initial velocities for a given impurity strength. These have not been observed during our simulations of the discrete topological chain. Instead, we only observe a small range of alternating regimes where the antikink is transmitted or trapped, around $k_i/k = 0.75$ and $v_0 = 3.6$ in Fig. 3.4b. We leave a detailed
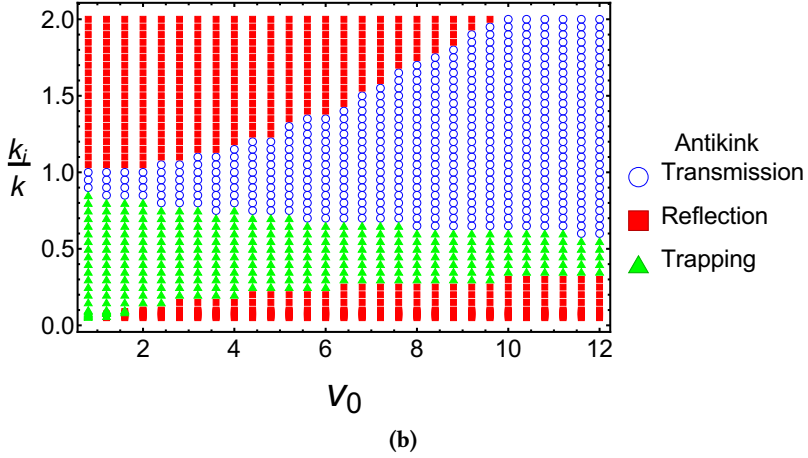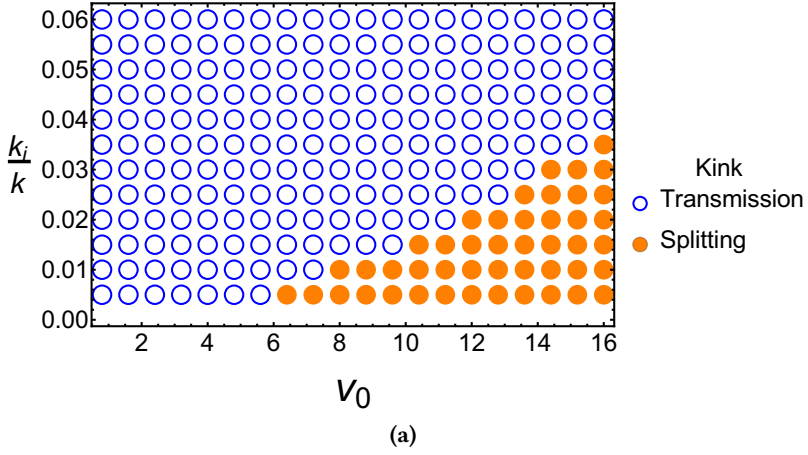
(a)

(b)

Figure 3.4. The phase diagram of the scattering behavior in the parameter space of normalized spring stiffness constant of impurity k_i/k and kink initial velocity v_0 for (**a**) the kink and (**b**) the antikink. The system parameters are the same as Fig. 3.2. The lower limit of v_0 for the antikink is around 0.7, below which even the PN barrier in a perfect chain will capture the antikink.

characterization of the resonance energy exchange between these modes for future studies.

3.2 Spring length impurities

In Sec. 2.4 we perform linear mode analysis of the topological chain, and in Sec. 3.1 we study the nonlinear motion of (anti)kinks with impurities. Here in this section we will show in a qualitative way that there is a connection between these two aspects. For convenience, we investigate another type of impurity: the spring length.

3.2.1 Linear mode analysis

We start with a qualitative observation of the linear vibrational modes. For a perfect topological rotor chain with free boundary conditions, there exists only one zero mode – the translation mode of the kink. This is what the Maxwell-Calladine counting predicts [57, 58]: the chain has n rotors as degrees of freedom and $n - 1$ springs as constraints, and the former quantity minus the latter equals the number of zero modes minus the number of states of self stress. (In a perfect chain there is no states of self stress.) This counting does not depend on the geometrical parameters of the chain components.

Now we increase one geometrical parameter, namely the length of the middle spring l_0, so that it is an impurity in the system (Fig. 3.5). As long as no state of self stress is created, there remains only one zero mode. However, as l_0 approaches a critical value $l_{critical}$, several qualitative changes take place: (1) The profile of the chain varies significantly. There are two kinks, one on each side of the impurity spring. (2) Eigenmode analysis shows that the amplitude of the zero mode has two prominent parts that are spatially separated, each of which is localized around a kink as an individual translation mode. Both parts of the zero mode point towards the same direction. (3) An additional soft vibrational mode appears, whose amplitude also has two separated parts just like the zero mode. But the directions of these two parts are opposite to each other. This soft mode has a frequency close to zero, much lower than that of kink shape modes. (4) A soft tensional mode dual to the soft vibrational mode emerges, being localized around the impurity spring. (A tensional mode is a vector whose components are the infinitesimal spring tensions caused by the infinitesimal motion of the dual vibrational mode. The duality comes from the fact that the tensional mode is an eigenfunction of the

supersymmetrical "partner" of the dynamical matrix, while the vibrational mode is an eigenfunction of just the dynamical matrix. See [19, 25, 26] for more details.)

These changes do not contradict the Maxwell-Calladine counting: only one vibrational mode has strictly zero frequency, unless l_0 actually reaches $l_{critical}$. In that case, the frequencies of both the soft vibrational mode and the soft tensional mode go to zero. By definition the tensional mode becomes a state of self stress. Then the Maxwell-Calladine counting still holds as there are now two zero modes and one state of self stress.

The above analysis only considers infinitesimal oscillations around zero-energy equilibrium points. In the next section, we study qualitatively the nonlinear motion of kinks with finite energy, providing a perspective complementary to the linear analysis.

3.2.2   Nonlinear dynamics: linkage limit

3.2.2.1   Setup: Hamiltonian

To simplify the problem, we consider the linkage limit, where all the springs in a perfect chain are non-deformable rigid bars so that they are holonomic constraints. There is only one degree of freedom which is the translational motion of the kink. We choose the kink position x as a collective variable to describe this degree of freedom.

Then we introduce the impurity by replacing the middle rigid bar with a longer spring that is "soft" (i.e. with a finite spring stiffness constant) (Fig. 3.6a). A soft spring does not strictly constrain the angles of the two rotors it connects but rather gives a potential energy to deviations from its preferred length. The chain then has one fewer constraint, which in turn means that it has two degrees of freedom. We regard the whole chain as two linkage sub-chains, then the two degrees of freedom are shared by the two kinks of the sub-chains, which we call Kink 1 and Kink 2 with position x_1 and x_2 respectively. The coordinate system for the discrete chain model is illustrated in Fig. 3.6a, and its precise definition is contained in Appendix 3.A. We see that by taking the linkage limit, the number of degrees of freedom is reduced from the number of rotors (16 for the chain in Fig. 3.6a) to the number of kinks (2 for two kinks).
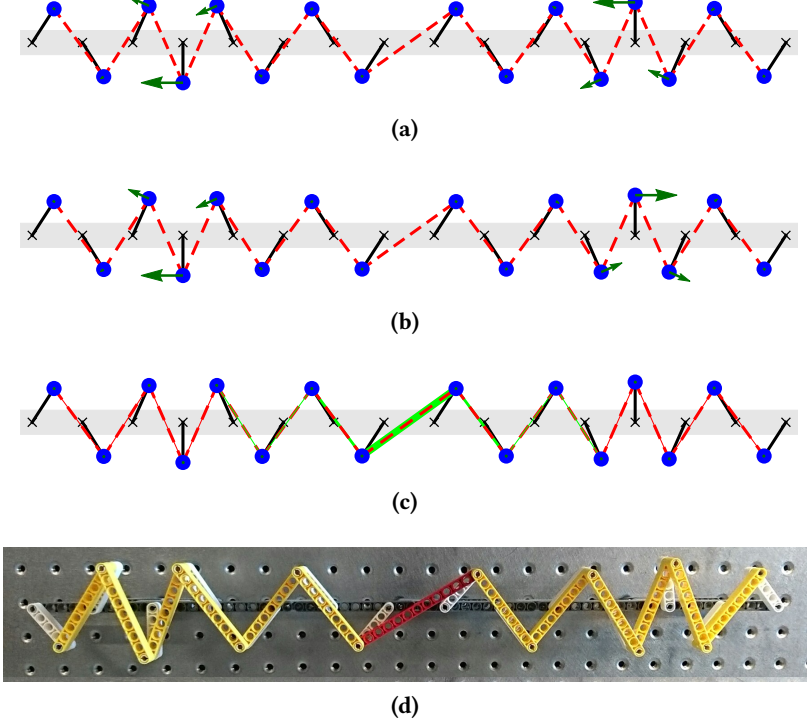
(a)

(b)

(c)

(d)

Figure 3.5. The zero vibrational mode (**a**), the soft vibrational mode (**b**), and the soft tensional mode (**c**) of a topological chain with a longer spring in the middle as an impurity. The configuration parameters are $\bar{\theta} = 0.58$, $r/a = 0.8$, $\bar{l}/a = 1.68$, $l_0/a = 2.30$ and $l_{critical}/a = 2.31$. The soft mode frequency is 7.7×10^{-9} in the unit of $(r/a)\sqrt{k/M}$, which means the mode is much "softer" than the kink shape mode whose frequency is of the order 10^{-2}. In (**a**) and (**b**), the arrows indicate the mode amplitude of the displacement of each rotor. In (**c**), the thickness of the green bars indicates the tensional mode amplitude on each spring. All the springs, both normal ones and the impurity, have the same stiffness. (**d**) shows a LEGO demonstration.
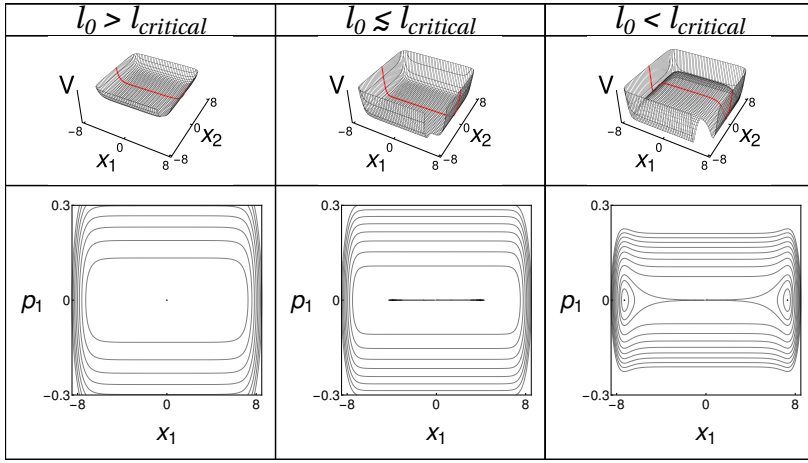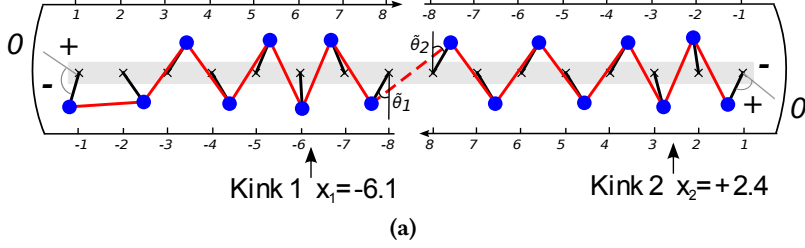
(a)

(b)

Figure 3.6. (a) Illustration of the coordinate system of a topological rotor linkage chain with $\bar{\theta} = 0.58$, $r/a = 0.8$, $\bar{l}/a = 1.68$ and $l_{critical}/a = 2.31$. The linkage bars are the solid lines and the impurity spring is the dashed line. In **(b)**, the upper panels show the potential functions in 2D configuration space for various l_0. One corner of the function is trimmed for visualization. The red curve corresponds to the potential for Kink 1 in the one d.o.f. case where Kink 2 is fixed at $x_2 = 0$. The lower panels show the phase portraits of Kink 1.

Now we derive the Hamiltonian. Note that the potential energy only comes from the deformation of the impurity spring, which in turn just depends upon the angles of the head rotors $\tilde{\theta}_i$. Since x_i is the degree of freedom, it determines the state of the sub-chain i, including $\tilde{\theta}_i$. Thus from the continuum theory (Eq. 2.13 where $u = r \sin \theta$), we obtain $\tilde{\theta}_i(x_i)$:

$$\sin \tilde{\theta}_i(x_i) = \sin \overline{\theta} \tanh \left(\frac{r \sin \overline{\theta}(|x_i| - \tilde{x}_i)}{a^2} \right), \tag{3.1}$$

where $\overline{\theta}$ is the equilibrium angle of a perfect chain, a is the lattice spacing, r is the rotor length, and $\tilde{x}_i$ is the position of the head rotor.

Putting $\tilde{\theta}_i(x_i)$ into the Hookean spring potential $V = \frac{1}{2}k(l_{1,2} - l_0)^2$ where $l_{1,2}$ takes the form in Eq. (2.6) and l_0 is the rest length of the impurity spring, we obtain the potential function $V(x_1, x_2; l_0)$ as a function of the kink positions (Fig. 3.6b). We formally define the effective kink momentum p and mass m for the sub-chains in terms of the total kinetic energy of the rotors $T = \sum_{j=1}^{8} \frac{1}{2}mr^2\dot{\theta}_j^2 \equiv \frac{1}{2m}p^2$. Thus the Hamiltonian $H(x_1, x_2, p_1, p_2; l_0) = T(p_1, p_2) + V(x_1, x_2; l_0)$ is obtained.

3.2.2.2   Individual kink: Phase portrait

We first investigate a simple case where Kink 2 is fixed at $x_2 = 0$ and only Kink 1 is allowed to move. Then the chain has only one degree of freedom x_1. With the Hamiltonian, we draw the phase portraits of x_i for various l_0 in Fig. 3.6b. We find that there is a critical value for the rest length of the impurity spring

$$l_{critical} = \sqrt{(2r \sin \overline{\theta} + a)^2 + (2r \cos \overline{\theta})^2}, \tag{3.2}$$

which determines the pattern of the phase portrait and the qualitative behavior of the dynamics of the chain.

When $l_0 < l_{critical}$, the dumbbell-shaped separatrix curve extends almost across the whole reachable region of x_1. The two equilibrium points at $x_1 \approx +8$ and $x_1 \approx -8$ correspond to the kink being localized around the impurity spring. x_1 is either positive or negative depending on the orientation of the end rotor. At these two equilibrium points the impurity spring is not stretched.

The behavior of Kink 1 depends on whether E is above or below the separatrix curve's energy $E_c = \frac{1}{2}k(l_0 - l_{critical})^2$. If $E < E_c$, the trajectory in the phase plane stays inside the region enclosed by separatrix and circulates around one of the equilibrium points. In real space, Kink 1 makes small oscillations around the impurity spring at either $x_1 \approx -8$ or $x_1 \approx +8$. If $E > E_c$ the trajectory moves in the region outside of the separatrix. In real space, Kink 1 is able to go over the sub-chain end and move back and forth between $x_1 \approx -8$ and $x_1 \approx +8$.

When l_0 approaches $l_{critical}$ from below and exceeds $l_{critical}$, the separatrix curve shrinks and disappears. The two equilibrium points merge into one at $x_1 = 0$ at the end of the sub-chain [1]. In real space, the kink with finite energy oscillates around the sub-chain end $x_1 = 0$.

3.2.2.3   Two kinks: Accessible configuration space

The phase space of a chain with two kinks is 4D. For the convenience of visualization, we investigate the potential function $V(x_1, x_2; l_0)$ in the 2D configuration space. The shape of the potential depends on l_0 and determines the qualitative dynamics of the two kinks. We also perform simulations of Newtonian dynamics to investigate the qualitative behavior of the nonlinear motion of the kinks.

When $l_0 < l_{critical}$ (Fig. 3.7a), the potential looks like a square Mexican hat. The bottom of potential valley is a square ring, on which all the points are at zero energy. In linear mode analysis, we find a zero mode along the valley and a soft mode along the transverse direction. We will show that the nonlinear dynamics at finite energy possesses the traits that are closely related to those in the linear analysis at zero energy.

Note that the impurity spring is maximally stretched at $x_1 = x_2 = 0$, and the corresponding potential maximum $E_c = \frac{1}{2}k(l_0 - l_{critical})^2$. It is the minimal energy for both kinks to move away from the impurity. If $E < E_c$, the two kinks take turns moving on their respective sub-chains. One kink oscillates near the impurity spring, while the other kink moves away. The nonlinear dynamics of the kinks is visualized as a trajectory going along the

---

[1]In the language of dynamical systems, this process is called a *supercritical pitchfork bifurcation*.
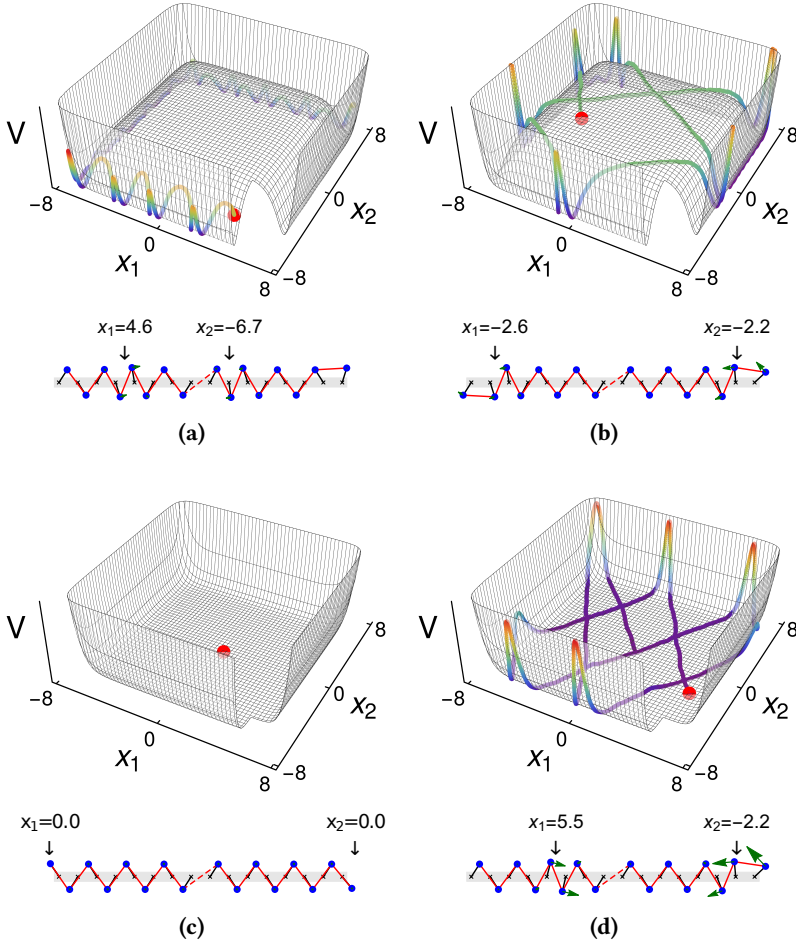
Figure 3.7. The trajectories of the chain generated by simulations of Newtonian dynamics on the theoretical potential function in the configuration space at **(a)** $l_0 < l_{critical}$, $E < E_c$, **(b)** $l_0 < l_{critical}$, $E > E_c$, **(c)** $l_0 = l_{critical}$, $E = E_c = 0$, and **(d)** $l_0 > l_{critical}$. In the top figures of **(a)** and **(b)**, the color scale of the trajectories indicates the potential energy of the chain in arbitrary units. The big red dots correspond to the configuration of the real-space chains shown in the bottom figures of each panel.

bottom of the potential valley. The accessible region in the configuration space is a square annulus, at the corner of which the major part of energy is transferred from the one kink to another. In fact, this can be interpreted as the motion of a single "split" kink through the system.

When $E \geq E_c$ (Fig. 3.7b), there is sufficient energy for both kinks to move away from the impurity spring simultaneously. In the configuration space, the trajectory gets out of the potential valley and climbs up to the 2D plateau in the middle. The accessible region now is a square disk. In real space, the kinks independently hit the impurity spring and get reflected.

When $l_0 = l_{critical}$ (Fig. 3.7c), the linear mode analysis predicts that the chain model in Fig. 3.7c has two zero modes, each being localized around the kink at the end of the respective sub-chain, and a state of self stress localized around the impurity spring. From the viewpoint of nonlinear dynamics, the potential function changes qualitatively: As l_0 approaches $l_{critical}$, the square ring of the potential valley shrinks into one point at $x_1 = x_2 = 0$, and E_c goes to zero. In other words, the Mexican hat transforms into a single basin. In this shrinking process, the soft mode, which corresponds to the oscillation transverse to the valley, transitions into a zero mode, because the depth of the valley vanishes. In terms of nonlinear dynamics, this transition means that no matter how small the total energy E is, the accessible region in the configuration space is always a square disk rather than a square annulus.

When $l_0 > l_{critical}$ (Fig. 3.7d), the impurity spring is compressed, which gives a minimum potential energy $E_{min} = \frac{1}{2}k(l_0 - l_{critical})^2$ for the static configuration. In a linear analysis, the two zero modes become normal modes with finite frequency, as the impurity spring pushes the two kinks to the chain ends, generating a finite restoring force for the motion of the modes. In the nonlinear dynamics, the accessible region of the kinks is still a square disk.

Fig. 3.8 summarizes the above results with E and l_0 as parameters. When $l_0 \leq l_{critical}$, the curve $E_c = \frac{1}{2}k(l_0 - l_{critical})^2$ marks the transition of the accessible region in configuration space from an annulus to a disk. Note that we only investigate the case of $l_0 > \bar{l}$, in which Fig. 3.8 is valid. For $l_0 < \bar{l}$ case, the potential landscape takes a different form, and so does the possible transition. We do not cover this case in this paper, however, as we have made the connection between linear mode analysis and nonlinear dynamics.
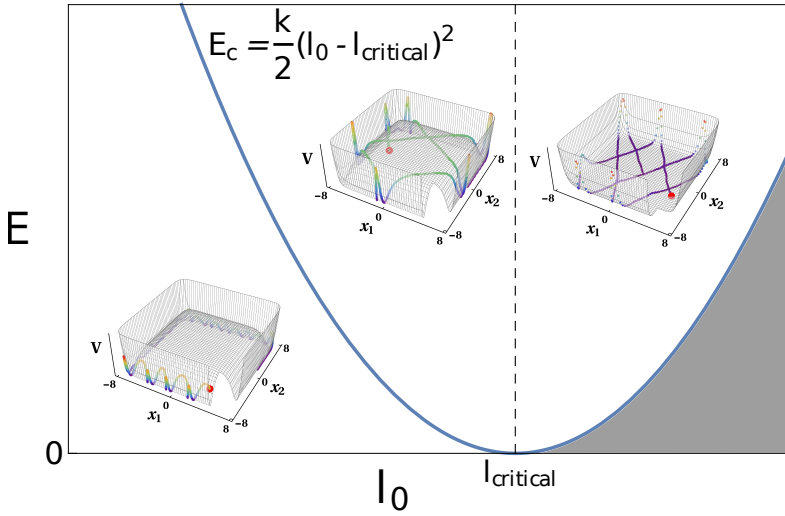
Figure 3.8. The parameter space of the total energy E and the impurity spring length l_0. The critical energy E_c as a function of l_0 forms a parabola. The chain shows different dynamical behaviors across the left branch of the parabola. The vertical dashed line of $l_0 = l_{critical}$ is the boundary line across which the shape of the potential function transitions qualitatively. The gray area below the right branch of the parabola is energetically forbidden.

Appendix

3.A Convention of kink coordinates in discrete models

The concept of kinks stems from the continuum ϕ^4 theory. To extend this concept to the discrete chain model, we define the coordinate system of a sub-chain kink as follows (Fig. 3.6a): The absolute value of the position of a kink equals the rotor's integer index if the rotor is vertical, otherwise the position is a real number interpolating between the indices of the two neighboring rotors that are leaning opposite to each other. The positional interpolation is proportional to the linear interpolation between the absolute values of the

angles of two neighbor rotors. The rotor angles are the measured against the vertical alternatively, as mentioned in Sec. 2.2. When a kink approaches the end points of the chain, the end rotor flips over. Here the kink profile from the continuum theory ceases to be valid. Thus we take as our convention that a kink is at the origin of the coordinate system when the end rotor is collinear with the spring connecting to the next rotor, and its sign depends on whether the end rotor leans upwards or downwards. The coordinate between 0 and 1 (or -2) is obtained by linear interpolation of the angles of the end rotor at 0 and 1 (or -2). In this *ad hoc* convention, the chain forms a state of self stress when both kinks are at origin. The two sub-chains are aligned head-to-head, and the two head rotors ($|x_i| = 8$) are coupled by the impurity spring.